

Interaction Models for GRB Afterglows

Zhi-Yun Li and Roger A. Chevalier

Department of Astronomy, University of Virginia, Charlottesville, VA 22903, USA

Abstract. We review interaction models for GRB afterglows, with an eye on constraining the nature of their progenitors and the geometry of explosion. Evidence is presented for two types of progenitors. The radio afterglow of GRB 980425/SN 1998bw and the multi-frequency observations of GRB 970508 can be fitted by a blast wave expanding into a wind-type medium, pointing to a massive star progenitor. The broadband afterglow data of GRBs 990123 and 990510 are better modeled by a jet expanding into a constant-density medium, implying a compact star merger origin. Among other well observed GRBs, the jet model appears to be more widely applicable than the wind model, although some cases are ambiguous. The model fits often require a deviation of the energy distribution of the radiating electrons from the commonly assumed single power-law form, particularly for sources with a rapid decline and/or pronounced steepening in the optical light curves. Transition to non-relativistic evolution has been suggested as an alternative explanation for the light curve steepening, although to produce steepening on the order of days or less would require very high ambient densities, which are generally difficult to reconcile with radio observations. Major open issues include the hydrodynamics of jet-ambient medium interaction, a self-consistent determination of the electron energy distribution, and the effects of pair production on the early afterglows which are expected to be particularly large for the wind interaction model.

1 Introduction

The simplest model of the afterglows of gamma-ray bursts (GRBs) involves a spherical relativistic blast wave expanding into a constant-density, presumably interstellar, medium [58,71]. The afterglows are emitted by nonthermal electrons accelerated at the shock front to an energy distribution usually assumed to be a power law above some cutoff determined by the shock velocity. The predicted power-law decay of the afterglow emission with time was subsequently observed at X-ray [20] and optical [113] wavelengths for GRB 970228, giving basic confirmation to this now “standard” picture [116,125].

To date, nearly 50 GRB afterglows have been observed at more than one frequency (for reviews of afterglow observations see Chapters by Piro, Pian & Fruchter, and Weiler). A dozen or so of these are well observed at multiple frequencies to allow for detailed modeling. Some features of these afterglows turn out to be difficult to accommodate in the standard model. The most noticeable is the relatively steep decline of the optical light curves, sometimes preceded by flatter evolution. The steep decline is usually attributed to a collimated or jet-like, rather than spherical, initial energy injection [96,105]. Alternatively, it could

be due to the transition of blast wave evolution to the non-relativistic regime [26], a non-standard electron energy distribution [66,78], and/or expansion into a wind-type ambient medium [18]. The question of a wind versus a constant-density surrounding medium is a crucial one for the progenitors of GRBs, since massive stars, one of the leading candidates for GRB progenitors [127,77], should be surrounded by a wind. In contrast, GRBs resulted from compact star mergers, the other leading candidate, are expected to be surrounded by the general interstellar medium (see Chapter by Waxman).

The plan of the Chapter is as follows. In § 2, we discuss the likely environments of GRBs relevant to afterglow evolution. In § 3, we outline the basics of various ambient interaction models for GRB afterglows. These models are then applied to individual GRBs with relatively well-observed afterglows (§ 4). We find that some of the sources are probably wind-interactors, while others are better modeled as interacting with a constant-density medium. This and other results are discussed in § 5.

2 The Ambient Medium

Models for the GRB afterglows indicate that the emission comes from a region $\sim 10^{16} - 10^{18}$ cm from the source of the explosion. The nature of the material in this region depends on the GRB progenitors, which are presently not known. There are two main possibilities. In one model, the progenitors are massive stars at the end of their lives [127,77]. In this case, the interaction is expected to be primarily with the mass loss from the progenitor leading up to the explosion. The other class of object is the merger of two compact objects for which there are a number of possibilities [38]. In this case, there may be some debris from the merger, but the interaction is expected to be primarily with the ISM (interstellar medium). We consider these possibilities in turn.

If the progenitors are massive stars, there is an analogy to the explosions of core collapse supernovae, for which there is abundant evidence that they are interacting with the winds from the progenitor stars (see Chapter by Chevalier & Fransson). In general, the interaction appears to be with the free wind from the progenitor star, with density $\rho_w = \dot{M}/(4\pi r^2 v_w)$, where \dot{M} is the mass loss rate from the star and v_w is the wind velocity. In most of the supernova cases, the radial range that is observed is out to a few 10^{17} cm, so that the mass loss characteristics have not substantially changed during the time that mass is supplied to the wind and $\rho_w \propto r^{-2}$. The density in the wind depends on the type of progenitor. Red supergiant stars, which are thought to be the progenitors of most Type II supernovae, have slow dense winds. Wolf-Rayet stars, which are thought to be the progenitors of Type Ib and Ic supernovae, have faster, lower density winds. SN 1987A is a special case in which the star was a red supergiant, but became a blue, B3 supergiant about 10^4 years before the explosion (see Chapter by McCray). The result was a complex circumstellar medium, including a dense ring at a radius of 6×10^{17} cm.

If GRBs do have massive star progenitors, there are a number of arguments suggesting that Wolf-Rayet stars are the most likely progenitors: (1) SN 1998bw, the best case of a SN – GRB association (GRB 980425), was of Type Ic, with a probable Wolf-Rayet progenitor. (2) The high energy of GRBs suggest that a moderately massive black hole is involved, which, in turn, requires a massive, $\gtrsim 20 - 25 M_\odot$, progenitor [29]. These stars are likely to be Wolf-Rayet stars at the end of their lives [44]. (3) The relativistic flow from a central object may be able to penetrate a relatively compact Wolf-Rayet star, but probably cannot penetrate an extended red supergiant star [68]. (4) If a rapidly rotating black hole is required for the GRB explosion, a merger at the center of a massive star is one way to obtain a rapidly rotating core. The merger process can give rise to a Wolf-Rayet star. None of these arguments is definitive, but they do point toward the most plausible progenitors.

The circumstellar medium created by a $35 M_\odot$ initial mass star that passes through a Wolf-Rayet phase and a prior red supergiant phase has been simulated by Garcia-Segura et al. [44]. They find that during the Wolf-Rayet phase, a broken shell is created at a radius of a few pc or more. This type of shell has been observed around a number of Wolf-Rayet stars. Inside of the shell is a region of shocked wind, with an approximately constant density [16]. The size of the shocked region is determined by what is required to decelerate the wind and is typically less than half of the shell radius. In general, the wind ram pressure $p = \rho_w v_w^2$ determines the size of the wind bubble that is created. The pressure is $p/k = 3.6 \times 10^9 \dot{M}_{-5} v_8 r_{17}^{-2} \text{ cm}^{-3} \text{ K}$, where $\dot{M}_{-5} = \dot{M}/10^{-5} M_\odot \text{ yr}^{-1}$, $v_8 = v_w/10^8 \text{ cm s}^{-1}$, and $r_{17} = r/10^{17} \text{ cm}$. For comparison, the interstellar pressure in the solar neighborhood is $\sim 3000 \text{ cm}^{-3} \text{ K}$. The region out to the wind termination shock can be described by a density $\rho_w = 5 \times 10^{11} A_* r^{-2} \text{ g cm}^{-3}$, where $A_* = 1 \dot{M}_{-5} v_8^{-1}$. Considering the radial range relevant to GRB afterglows, we expect this to apply to most cases, unless the wind is especially weak or the surrounding pressure is extraordinarily high. Ramirez-Ruiz et al. [92] have followed the circumstellar mass loss from Wolf-Rayet stars and found that the free wind does not extend to large radii in their treatment.

For bursts that interact directly with the ISM, the size scale of the afterglows suggests that the medium has a roughly constant density, although the ISM is known to have considerable density inhomogeneity on a range of scales. The range of interstellar densities in a galaxy like our own goes from $\sim 10^{-3} \text{ cm}^{-3}$ in the hot ISM to $\gtrsim 10^6 \text{ cm}^{-3}$ in compact cores in molecular clouds. The high densities are found in a very small volume fraction so that a typical event is unlikely to occur in such a region. The situation may change in a starburst region, where a significant fraction of the gas may have a density $\gtrsim 10^3 \text{ cm}^{-3}$ [107]. The radio-bright, compact supernova remnants in starburst regions may be interacting with this dense interstellar component [15]. The finding that GRB 010222 may have occurred within a very active starburst [36] indicates that the interstellar environments of GRBs may have unusual properties.

Although the interstellar and wind models are the two main types of environments considered for afterglows, there is a different scenario involving a massive

star, motivated by the observation of possible Fe lines in the X-ray spectra of afterglows [88,128,89,2]. The observations appear to require a substantial mass of Fe at $r \sim 10^{16}$ cm, so one suggestion is that a supernova occurs before a GRB and that the ejecta have time to expand to this radius [114]. This requires that the GRB be delayed by months. The supernova would expand into the progenitor wind, creating a complex circumburst region in the inner part of the wind.

3 Ambient Interaction Models

3.1 Standard ISM-Interaction Model

We start with the simplest model of GRB afterglows involving synchrotron emission from a spherical relativistic blast wave propagating into a constant-density interstellar medium. The model was worked out in some detail by Mészáros & Rees [71] in advance of the afterglow detection. It has since been elaborated upon by others (e.g., [116,117,124]), and in particular [106]. Here, we will follow the formalism of Sari et al. [106], which has been widely used to interpret the spectra and light curves of GRB afterglows. This standard model serves as a benchmark against which other models will be compared.

The standard model assumes that the synchrotron-emitting electrons are accelerated at the shock front to a power-law distribution of Lorentz factor $N(\gamma_e) d\gamma_e \propto \gamma_e^{-p} d\gamma_e$ (with $p > 2$) above some minimum cutoff γ_m , which is determined by the shock velocity. This distribution is further modified by synchrotron cooling in the downstream flow. Denote by γ_c the Lorentz factor of an electron which cools in a blast wave expansion time. In the “fast cooling” case with $\gamma_c < \gamma_m$, the electron distribution is given by γ_e^{-2} between γ_c and γ_m and γ_e^{-p-1} above γ_m . This electron distribution produces a synchrotron spectrum of the flux $F_\nu \propto \nu^{-1/2}$ between ν_c and ν_m , the characteristic frequencies of the photons produced by electrons with γ_c and γ_m respectively, $F_\nu \propto \nu^{-p/2}$ above ν_m , and $F_\nu \propto \nu^{1/3}$ below ν_c . The spectrum is modified by synchrotron self-absorption, which typically occurs at relatively low frequencies. Assuming that the self-absorption frequency ν_a is less than the cooling frequency ν_c and that the absorbing electrons that have cooled for different lengths of time are well mixed spatially [48], we have $F_\nu \propto \nu^2$ below ν_a . In the opposite, “slow cooling” case with $\gamma_c > \gamma_m$, the electron distribution steepens to γ_e^{-p-1} above γ_c . Assuming that the self-absorption frequency ν_a is less than the characteristic frequency ν_m , we have the following spectrum: $F_\nu \propto \nu^2$ for $\nu < \nu_a$, $F_\nu \propto \nu^{1/3}$ for $\nu_a < \nu < \nu_m$, $F_\nu \propto \nu^{-(p-1)/2}$ for $\nu_m < \nu < \nu_c$, and $F_\nu \propto \nu^{-p/2}$ for $\nu > \nu_c$. These broken power-law expressions are often used to interpret the instantaneous spectra of GRB afterglows. They tend to agree with the more accurately determined spectra to within a factor of a few (e.g., [47]).

To obtain light curves, one must first determine the time evolution of the characteristic frequencies (ν_a , ν_m and ν_c) and the peak flux $F_{\nu,\max}$. The evolution depends on the dynamics of the blast wave. For the spherical blast wave propagating into a constant-density medium envisioned in the standard model,

the dynamics are described by the self-similar solutions of Blandford & McKee [8]: the blast wave Lorentz factor γ varies with the distance R from the explosion center as $\gamma \propto R^{-3/2}$ in the adiabatic regime and $\gamma \propto R^{-3}$ in the fully radiative regime. The Lorentz factor and distance are related to the detector-time t as $t \propto R/\gamma^2$. Making the standard assumption that a constant fraction ϵ_e (ϵ_B) of the blast wave energy goes into the electrons (magnetic fields) and making use of the jump conditions for relativistic shocks, one obtains the following scalings: $\nu_a \propto t^0$, $\nu_m \propto t^{-3/2}$, $\nu_c \propto t^{-1/2}$, and $F_{\nu, \max} \propto t^0$ for the slow cooling case, which is always in the adiabatic regime. In the fast cooling case, if the electron energy fraction ϵ_e is close to unity, then the blast wave is fully radiative, and the scalings become: $\nu_a \propto t^{-4/5}$, $\nu_c \propto t^{-2/7}$, $\nu_m \propto t^{-12/7}$, and $F_{\nu, \max} \propto t^{-3/7}$. If on the other hand $\epsilon_e \ll 1$, the evolution remains adiabatic, and the scalings are the same as in the slow cooling case, except for the self-absorption frequency which now decreases with time as $\nu_a \propto t^{-1/2}$. These scalings are combined with the instantaneous spectra listed above to obtain light curves.

The light curve at a given observing frequency ν can be described by a broken power-law with breaks at various characteristic times. These include the times t_a , t_m and t_c when the characteristic frequencies ν_a , ν_m and ν_c pass, respectively, the observing frequency ν . Ignoring self-absorption, Sari et al. [106] obtained two types of light curves in two frequency regimes, separated by a critical frequency ν_0 at which the characteristic times t_m and t_c become equal, i.e., $t_m(\nu_0) = t_c(\nu_0) \equiv t_0$. The critical time t_0 divides the early, fast cooling part of the light curve from the later, slow cooling part. In the high frequency regime where $\nu > \nu_0$, the ordering of the characteristic times is $t_c < t_m < t_0$, which yields a light curve of $F_\nu \propto t^{1/6}$ for $t < t_c$, $F_\nu \propto t^{-1/4}$ for $t_c < t < t_m$, and $F_\nu \propto t^{(2-3p)/4}$ for $t > t_m$ in the case of adiabatic evolution. In the opposite case of fully radiative evolution, which is possible only before the critical time t_0 when the electrons are fast cooling, one has instead $F_\nu \propto t^{-1/3}$ for $t < t_c$, $F_\nu \propto t^{-4/7}$ for $t_c < t < t_m$, and $F_\nu \propto t^{(2-6p)/7}$ for $t_m < t < t_0$. In the low frequency regime where $\nu < \nu_0$, the ordering of the characteristic times becomes $t_0 < t_m < t_c$. The light curve is then $F_\nu \propto t^{1/6}$ for $t < t_0$, $F_\nu \propto t^{1/2}$ for $t_0 < t < t_m$, $F_\nu \propto t^{3(1-p)/4}$ for $t_m < t < t_c$, and $F_\nu \propto t^{(2-3p)/4}$ for $t > t_c$ in the adiabatic case. In the fully radiative case, one has $F_\nu \propto t^{-1/3}$ for $t < t_0$ instead.

Synchrotron self-absorption modifies the light curves. We will concentrate on the case of adiabatic evolution here and below; it is more likely than the fully radiative case during most of the afterglow phase of a GRB evolution (e.g., [71]). The self-absorption is characterized by the absorption frequency ν_a , which decreases with time as $\nu_a \propto t^{-1/2}$ during the fast cooling period $t < t_0$. It has a constant value, denoted by $\nu_{a,0}$, between $t_0 < t < t_{am}$, where t_{am} is another critical time when the characteristic frequencies ν_a and ν_m become equal. In the frequency regime $\nu > \nu_{a,0}$, both the high and low frequency light curves discussed above have an additional power-law segment $F_\nu \propto t$ before the characteristic time t_a , which is smaller than any other characteristic time. Collecting all time and frequency dependences, we finally have $F_\nu \propto t\nu^2$ ($t < t_a$), $F_\nu \propto t^{1/6}\nu^{1/3}$ ($t_a < t < t_c$), $F_\nu \propto t^{-1/4}\nu^{-1/2}$ ($t_c < t < t_m$), and $F_\nu \propto t^{(2-3p)/4}\nu^{-p/2}$ ($t > t_m$)

for the high frequency light curve, and $F_\nu \propto t\nu^2$ ($t < t_a$), $F_\nu \propto t^{1/6}\nu^{1/3}$ ($t_a < t < t_0$), $F_\nu \propto t^{1/2}\nu^{1/3}$ ($t_0 < t < t_m$), $F_\nu \propto t^{3(1-p)/4}\nu^{-(p-1)/2}$ ($t_m < t < t_c$), and $F_\nu \propto t^{(2-3p)/4}\nu^{-p/2}$ ($t > t_c$) for the low frequency light curve. The time and frequency dependences of the flux are sometimes parameterized using $F_\nu \propto t^\alpha\nu^\beta$. The relations between the decay index α and spectral index β , $\alpha = 3(1-p)/4 = 3\beta/2$ ($t_m < t < t_c$ or $\nu_m < \nu < \nu_c$) and $\alpha = (2-3p)/4 = (1+3\beta)/2$ ($t > t_c$ or $\nu > \nu_c > \nu_m$) in the most relevant, slow cooling case, are often used to interpret optical and X-ray afterglow observations at relatively late times (of order one day or more). In the frequency regime $\nu < \nu_{a,0}$, more relevant to radio afterglows, one has the ordering $t_0 < t_m < t_a < t_c$, which yields $F_\nu \propto t\nu^2$ ($t < t_0$), $F_\nu \propto t^{1/2}\nu^2$ ($t_0 < t < t_m$), $F_\nu \propto t^{5/4}\nu^{5/2}$ ($t_m < t < t_a$), $F_\nu \propto t^{3(1-p)/4}\nu^{-(p-1)/2}$ ($t_a < t < t_c$), and $F_\nu \propto t^{(2-3p)/4}\nu^{-p/2}$ ($t > t_c$). We reiterate that the scalings involving self-absorption in the fast cooling case with $t < t_0$ are derived assuming that the energy distribution of the cooling electrons is spatially homogeneous in the emission region behind the shock front. The opposite situation where layers of cooling electrons at different distances from the shock front remain unmixed has been considered in detail by Granot et al. [48] and Granot & Sari [49].

3.2 Wind-Interaction Model

The first modification of the standard model we consider is the density distribution of the ambient medium. Mészáros, Rees, & Wijers [74] studied the general case of a power-law ambient density distribution $n \propto r^{-s}$, with an arbitrary power-index s . Chevalier & Li [17,18] examined the specific case of $s = 2$, corresponding to a constant-mass loss rate, constant-velocity, circumstellar wind, possibly of a Wolf-Rayet origin. Some features of the wind-interaction model are also described in Dai & Lu [25] and Panaitescu, Mészáros & Rees [84]. Here, we follow the formalism of Chevalier & Li [18].

The wind-interaction model has the same instantaneous afterglow spectra as in the standard ISM-interaction model, but different light curves. The differences in light curve come from the blast wave dynamics. For a relativistic blast wave propagating in an $s = 2$ medium, Blandford & McKee [8] showed that its Lorentz factor $\gamma \propto R^{-1/2}$ in the adiabatic regime, and $\gamma \propto R^{-1}$ in the fully radiative regime. Concentrating on the adiabatic evolution as before and making the standard assumption about the fractions of the blast wave energy going into the electrons and magnetic fields, one finds that the characteristic frequencies scale with time as $\nu_a \propto t^{-3/5}$, $\nu_m \propto t^{-3/2}$, and $\nu_c \propto t^{1/2}$, and the peak flux $F_{\nu,\max} \propto t^{-1/2}$ in the slow cooling case. In the fast cooling case, the scalings are the same except for the self-absorption frequency, which now decreases with time more rapidly as $\nu_a \propto t^{-8/5}$.

The above scalings of the characteristic frequencies define four critical times, with four corresponding critical frequencies which divide the light curves into five distinct frequency regimes. For the typical parameters adopted by Chevalier & Li [18], the light curve that is most relevant to the optical and X-ray afterglows has the ordering $t_a < t_m < t_0 < t_c$, which yields $F_\nu \propto t^{7/4}\nu^{5/2}$ for $t < t_a$, $F_\nu \propto t^{-1/4}\nu^{-1/2}$ for $t_a < t < t_m$, $F_\nu \propto t^{(2-3p)/4}\nu^{-p/2}$ for $t_m < t < t_0$, $F_\nu \propto$

$t^{(2-3p)/4}\nu^{-p/2}$ for $t_0 < t < t_c$, and $F_\nu \propto t^{(1-3p)/4}\nu^{-(p-1)/2}$ for $t > t_c$. Note that as the cooling frequency ν_c moves across the observing frequency ν from below, the light curve steepens from $\alpha = (2 - 3p)/4$ to $(1 - 3p)/4$ by a modest amount $\Delta\alpha = 1/4$. The same amount of steepening, from $\alpha = 3(1 - p)/4$ to $(2 - 3p)/4$, also occurs in the standard ISM-interaction model, as ν_c moves across ν from above. A signature of the wind-interaction model is the relatively fast decline of the light curve in the non-cooling spectral region $\nu_m < \nu < \nu_c$, where $\alpha = (1 - 3p)/4$ compared with $3(1 - p)/4$ for the ISM case. If the cooling frequency falls between optical and X-ray wavelengths, the wind model would predict an X-ray light curve declining less steeply than an optical light curve, whereas the opposite would be true for the ISM model.

At the much lower, radio frequency, the characteristic times typically have the following ordering: $t_c < t_0 < t_a < t_m$, which leads to a light curve with $F_\nu \propto t^{7/4}\nu^{5/2}$ for $t < t_c$, $F_\nu \propto t^2\nu^2$ for $t_c < t < t_0$, $F_\nu \propto t\nu^2$ for $t_0 < t < t_a$, $F_\nu \propto t^0\nu^{1/3}$ for $t_a < t < t_m$, and $F_\nu \propto t^{(1-3p)/4}\nu^{-(p-1)/2}$ for $t > t_m$. In the slow cooling case with $t > t_0$ most relevant to radio observations, the fairly steep rise of radio flux $F_\nu \propto t$ at the self-absorbed frequencies could in principle distinguish the wind model from the standard ISM model, where the rise is slower ($F_\nu \propto t^{1/2}$). In practice, the difference is masked to a large extent by interstellar scintillation.

3.3 Transition to Non-relativistic Evolution

After a GRB blast wave sweeps up a mass equivalent to the rest mass of the explosion, its evolution becomes non-relativistic. In a medium of constant density n , this happens at a radius of order $R_{\text{nr}} = 1.2 \times 10^{18} E_{52}^{1/3} n^{-1/3}$ cm where E_{52} is the explosion energy in units of 10^{52} ergs and n the ambient number density in units of cm^{-3} . The transition occurs on a time scale $t_{\text{nr}} = R_{\text{nr}}/c = 1.2(1 + z)E_{52}^{1/3} n^{-1/3}$ yr (where z is the cosmological redshift), which is longer than the typical duration of GRB afterglow observations, unless the explosion energy is much lower than 10^{52} ergs [33] and/or the density much higher than 1 cm^{-3} [26]. Provided that the minimum electron Lorentz factor $\gamma_m > 1$, the temporal and frequency dependences of the flux in the non-relativistic regime can be obtained in a way similar to that in the relativistic regime [125]. Here, we follow the detailed treatment of Frail et al. [33]. The electrons are typically slow cooling, with $\nu_m \propto t^{-3}$, $\nu_c \propto t^{-1/5}$, and the peak flux at ν_m given by $F_{\nu, \text{max}} \propto t^{3/5}$. The self-absorption frequency could either be greater or smaller than ν_m . There are two relevant orderings of characteristic frequencies: $\nu_a < \nu_m < \nu_c$ and $\nu_m < \nu_a < \nu_c$. In the former case, $\nu_a \propto t^{6/5}$, one has $F_\nu \propto \nu^2 t^{-2/5}$ for $\nu < \nu_a$, $F_\nu \propto \nu^{1/3} t^{8/5}$ for $\nu_a < \nu < \nu_m$, $F_\nu \propto \nu^{-(p-1)/2} t^{3(7-5p)/10}$ for $\nu_m < \nu < \nu_c$, and $F_\nu \propto \nu^{-p/2} t^{(4-3p)/2}$ for $\nu > \nu_c$. In the latter case, $\nu_a \propto t^{(2-3p)/(p+4)}$, and $F_\nu \propto \nu^2 t^{13/5}$ for $\nu < \nu_m$, $F_\nu \propto \nu^{5/2} t^{11/10}$ for $\nu_m < \nu < \nu_a$, $F_\nu \propto \nu^{-(p-1)/2} t^{3(7-5p)/10}$ for $\nu_a < \nu < \nu_c$, and $F_\nu \propto \nu^{-p/2} t^{(4-3p)/2}$ for $\nu > \nu_c$. Note that the light curve decreases with time faster in the non-relativistic regime (where $\alpha = 3[7 - 5p]/10$ and $[4 - 3p]/2$ before and after the cooling break t_c , or $\alpha = -1.65$ and -1.75 for

$p = 2.5$) than in the relativistic regime (where the corresponding $\alpha = 3[1 - p]/4$ and $[2 - 3p]/4$ or $\alpha = -1.125$ and -1.375).

In the wind interaction model with an ambient density $\rho = Ar^{-2}$, the transition to non-relativistic evolution occurs at a distance $R_{\text{nr}} = 1.8 \times 10^{18} E_{52}/A_*$ cm, where A_* is the coefficient A in units of 5×10^{11} g cm $^{-1}$ [18], corresponding to a time $t_{\text{nr}} = 1.9(1+z)E_{52}/A_*$ yr, again longer than most afterglow observations for typical parameters. In the non-relativistic regime, one finds $\nu_m \propto t^{-7/3}$, $\nu_c \propto t$, and the peak flux $F_{\nu, \text{max}} \propto t^{-1/3}$ at ν_m . The relevant orderings are $\nu_a < \nu_m < \nu_c$ and $\nu_m < \nu_a < \nu_c$. In the former case, $\nu_a \propto t^{13/15}$, and $F_\nu \propto \nu^2 t^{-1}$ for $\nu < \nu_a$, $F_\nu \propto \nu^{1/3} t^{4/9}$ for $\nu_a < \nu < \nu_m$, $F_\nu \propto \nu^{-(p-1)/2} t^{(5-7p)/6}$ for $\nu_m < \nu < \nu_c$, and $F_\nu \propto \nu^{-p/2} t^{(8-7p)/6}$ for $\nu > \nu_c$. In the latter case, $\nu_a \propto t^{(4-7p)/[3(p+4)]}$, and $F_\nu \propto \nu^2 t^{-1}$ for $\nu < \nu_m$, $F_\nu \propto \nu^{5/2} t^{1/6}$ for $\nu_m < \nu < \nu_a$, $F_\nu \propto \nu^{-(p-1)/2} t^{(5-7p)/6}$ for $\nu_a < \nu < \nu_c$, and $F_\nu \propto \nu^{-p/2} t^{(8-7p)/6}$ for $\nu > \nu_c$. As in ISM interaction, the light curve decreases with time faster in the non-relativistic regime (where $\alpha = [8 - 7p]/6$ and $[5 - 7p]/6$ before and after the cooling break t_c , or $\alpha = -1.58$ and -2.08 for $p = 2.5$) than in the relativistic regime (where the corresponding $\alpha = [2 - 3p]/4$ and $[1 - 3p]/4$ or $\alpha = -1.375$ and -1.625).

3.4 Jet Model

Starting with Rhoads [96], jet models of afterglows have been widely discussed in connection with the steepening of light curves. We will first outline the asymptotic analysis of Sari, Piran & Halpern [105] and then comment on possible complications. Recent reviews of the subject include [98] and [86].

Let θ_0 be the initial angular width of the jet. When the Lorentz factor γ drops below θ_0^{-1} , the jet starts to spread sideways, changing its dynamics. The spreading occurs around a time $t_{\text{jet}} = 3[(1+z)/2](E_{52}/n)^{1/3}(\theta_0/0.2)^{8/3}$ days in a constant-density medium and $t_{\text{jet}} = 2[(1+z)/2](E_{52}/A_*)(\theta_0/0.2)^4$ days in a wind [18]. Before t_{jet} , the standard spherical results apply. After t_{jet} , the jet Lorentz factor decreases with distance exponentially [96], yielding $\gamma \propto t^{-1/2}$, $\nu_m \propto t^{-2}$ and $\nu_c \propto t^0$, and the peak flux $F_{\nu, \text{max}} \propto t^{-1}$ at ν_m . In the case $\nu_a < \nu_m < \nu_c$, one finds that $\nu_a \propto t^{-1/5}$, and $F_\nu \propto \nu^2 t^0$ for $\nu < \nu_a$, $F_\nu \propto \nu^{1/3} t^{-1/3}$ for $\nu_a < \nu < \nu_m$, $F_\nu \propto \nu^{-(p-1)/2} t^{-p}$ for $\nu_m < \nu < \nu_c$, and $F_\nu \propto \nu^{-p/2} t^{-p}$ for $\nu > \nu_c$. In the case $\nu_m < \nu_a < \nu_c$, we have instead $\nu_a \propto t^{-2(p+1)/(p+4)}$, and $F_\nu \propto \nu^2 t^0$ for $\nu < \nu_m$, $F_\nu \propto \nu^{5/2} t$ for $\nu_m < \nu < \nu_a$, $F_\nu \propto \nu^{-(p-1)/2} t^{-p}$ for $\nu_a < \nu < \nu_c$, and $F_\nu \propto \nu^{-p/2} t^{-p}$ for $\nu > \nu_c$. These scalings apply to both ISM and wind interaction models.

The steepening of light curves to an asymptotic scaling of $F_\nu \propto t^{-p}$ is a signature of the jet models. How sharply the change from one temporal slope to another actually happens remains controversial. Mészáros & Rees [72] pointed out that seeing the edge of a jet when its Lorentz factor drops below θ_0^{-1} would also steepen the light curve, by a factor of $\Delta\alpha = 3/4$ in a constant-density medium and $\Delta\alpha = 1/2$ in a wind. Semi-analytic calculations taking into account of both the sideways spreading and edge effect find that the transition from one slope to another tends to be continuous, spanning one decade or more in the observer's time [76,120,62], especially in a wind-type ambient medium. These

calculations adopted a simplified set of 1D equations for the jet dynamics, which need to be checked against numerical simulations. Preliminary 2D calculations of Granot et al. [50] show that the blast wave has an egg-like shape, differing considerably from that predicted from the analytic or semi-analytic models. A steepening of light curves does occur around the time $\gamma \propto \theta_0^{-1}$, as expected from simple arguments. Whether the sharpness and amount of steepening match the predictions of the semi-analytic models remain to be seen.

3.5 Other Modifications

Many additional effects have been considered in the afterglow literature on top of the basic interaction models outlined above. We will limit ourselves to three of the more commonly discussed ones: inverse Compton scattering, pair production, and a non-standard electron energy distribution.

Inverse Comptonization of synchrotron photons by relativistic electrons could not only produce a high energy component of afterglow emission that is potentially observable but also dominate the cooling of electrons and affect the blast wave dynamics [83,119,19,79]. Sari & Esin [103] examined these effects in detail, and concluded that the inverse Compton spectra broadly resemble the primary synchrotron spectra in shape, although significant differences do exist, especially at the high frequency end where a broken power-law description is no longer adequate. They showed that as long as the fraction of the blast wave energy in electrons ϵ_e exceeds that in magnetic fields ϵ_B , the inverse Compton emission dominates the synchrotron emission in cooling the electrons in the fast cooling regime. Depending on the ratio ϵ_e/ϵ_B , the domination can extend well into the slow cooling regime, changing the value of the cooling frequency ν_c and thus the light curves of afterglow emission.

Thompson & Madau [112] considered pair formation as the gamma-ray photons from the GRB proper propagate ahead of the external shock front and interact with the seed photons back-scattered by the ambient medium. A simplified discussion of the process is presented in Mészáros, Ramirez-Ruiz & Rees [70]. Beloborodov [4] went one step further and solved for the dynamics of the pair-loaded medium. These studies concluded that pair production can dramatically increase the radiative efficiency of the blast wave and potentially broaden the original pulses of gamma-rays if the ambient density is high enough. The effects on afterglows are expected to be large at early times, especially for the wind-interaction model, although details are yet to be worked out.

Most afterglow models assume that the radiating electrons have a power-law energy distribution at injection above some cutoff. The power-law indexes inferred from afterglow observations under this assumption span a wide range, from $p \sim 2$ (or below) to ~ 3 (e.g., [18,80,81]). The lack of a universal value for p calls into question the assumption that the shock front accelerates electrons to a power-law that is constant with energy and with time. Indeed, in the Crab Nebula, arguably the best studied astrophysical synchrotron source, a break in the injection spectrum is required [1]. This motivated Li & Chevalier [66] to consider a broken power-law distribution of electron energy that steepens at

high energies in the context of the spherical wind-interaction model. Similar non-standard energy distributions have been adopted in other models [24,78,121]. A major attraction of the invoked steepening of electron energy distribution is that it can lead to a steepening of afterglow light curves. The light curve steepening is chromatic, and should be distinguishable from the achromatic steepening due to jet effects if wide wavelength coverage is available.

4 Application to Individual Sources

We now apply the interaction models to the dozen or so GRBs whose afterglows are relatively well observed. It turns out that for most of the sources the models are not unique. We shall start the discussion with the cases that in our view are less controversial.

4.1 Probable Collimated ISM Interactors: GRBs 990123 and 990510

The first two GRBs that show breaks in their optical afterglows are GRB 990123 [61] and GRB 990510 [52]. The breaks in both sources are achromatic and are interpreted as due to jets. In the case of GRB 990123, the break occurs at a time $t_b = 1.68 \pm 0.19$ days, depending somewhat on the fitting function adopted [55]. Before the break, the temporal decay index at optical wavelengths is $\alpha = -1.12 \pm 0.08$. The optical spectral index is found to be $\beta = -0.750 \pm 0.068$. These two indexes can be fitted by an ISM-interaction model with $p = 2.5$ in the adiabatic regime (where $\alpha = -3[p - 1]/4$ and $\beta = -[p - 1]/2$ for $\nu_m < \nu < \nu_c$). The decay index $\alpha = -1.44 \pm 0.07$ at X-ray wavelengths is also consistent with the model, provided that the X-rays are in the cooling regime (where $\alpha = [2 - 3p]/4$ for $\nu > \nu_c$). The observed steeper decline in X-rays than in optical is expected for ISM interaction but not for wind interaction [17]. After the break, the optical light curves steepen quickly to $\alpha = -1.69 \pm 0.06$ while the spectral index β remains approximately the same [55]. The observed amount of steepening, $\Delta\alpha = 0.57 \pm 0.10$, agrees marginally with that expected of a jet with a fixed opening angle (where $\Delta\alpha = 3/4$ for ISM interaction). It is less than half of the asymptotic value $\Delta\alpha = (p + 3)/4 = 1.38$ expected from the sideways expansion of a jet. The relatively small amount of steepening was taken as evidence for seeing the edge of a non-spreading jet [72,61,55], although it does not rule out jet-spreading as the cause of steepening, since it takes time for the light curves to reach the asymptotic slope. Indeed, Panaitescu & Kumar [80] obtained a reasonable fit to the multi-frequency data of GRB 990123 using a semi-analytic jet model taking into account of lateral expansion.

The breaks in the optical light curves of GRB 990510 appear to be smoother than those in GRB 990123. Fitting a continuous function, Harrison et al. [52] obtained a break time of $t_b = 1.20 \pm 0.08$ days. Before the break, the decay index $\alpha = -0.82 \pm 0.02$, which implies $p = 2.1$ in the adiabatic regime for ISM-interaction. The expected spectral index $\beta = -0.55$ is consistent with $\beta = -0.61 \pm 0.12$ determined by Stanek et al. [110] or $\beta = -0.531 \pm 0.019$ by Holland et

al. [55]. The latter authors find some evidence that β decreases with time which, if real, is not explained. The relatively flat decay rate of $\alpha > -1$ is difficult to accommodate in the wind-interaction model; it requires a very flat electron energy distribution with $p < 2$ [18]. Even then, the predicted spectral index would not match that observed [80]. After the break, the measured $\alpha = -2.18 \pm 0.05$, which is consistent with the expected asymptotic value $\alpha = -p$ [105]. The ISM-interacting jet model is further supported by radio data, which are consistent with the expected $F_\nu \propto t^{-1/3}$ evolution [52]. X-ray data are available between 0.3 and 2 days, bracketing the break in optical [64]. The lightcurve can be fitted either by single power-law with $\alpha = -1.42 \pm 0.07$ or a broken-power law, and is well modeled using an ISM-interacting jet model with the cooling frequency ν_c between the optical and X-rays [80,85]. The detection of polarization from this event [21,126] is also consistent with the jet interpretation [45,102], although the observed polarization is small and does not require a jet.

4.2 Probable Spherical Wind Interactors: GRBs 980425 and 970508

The probable association of GRB 980425 with the radio supernova SN 1998bw at $z = 0.0085$ is discussed in the Chapters by Galama and Iwamoto & Nomoto. Here, we are concerned with the radio emission from this source, which is extraordinary [61]. Kulkarni et al. [61] argued that the shock responsible for the radio emission is relativistic, based on the high brightness temperature, on a synchrotron self-absorption interpretation of the early evolution, and on scintillation results. Using the standard synchrotron theory, Li & Chevalier [65] were able to deduce from the radio data that the shock is expanding into a medium with an approximately r^{-2} density profile at a speed comparable to the speed of light. A more detailed model, taking into account of the shock dynamics and relativistic effects and assuming the standard power-law electron distribution above some cutoff, reproduces the radio lightcurves after about day 10 reasonably well, provided that the shock energy is increased by a factor of ~ 2.5 at $\sim 10^2$ days in the rest frame of the explosion to explain the rise in the radio fluxes observed between days 20–40. Based on the radio spectra at day 12 and day 15 and adopting a mono-energetic distribution for the synchrotron-emitting electrons, Waxman & Loeb [118] inferred a shock speed of $\sim 0.3 c$, which is a factor of ~ 2 smaller than that inferred by Li & Chevalier [65] around the same time. The longer term evolution of the radio source implies a power law particle energy distribution, as generally observed in GRB afterglows. Weiler, Panagia & Montes [122] were able to fit a parameterized model to the radio data, and came to a similar conclusion that the shock is mildly relativistic and is interacting with a clumpy progenitor wind.

Chevalier & Li [18] applied the spherical wind-interaction model to GRB 970508 which, unlike GRB 980425, is at a cosmological distance of $z = 0.835$ [75]. Extensive optical data up to hundreds of days are available for this source (see Chapter by Pian & Fruchter). They follow a power-law after about day 2 with $\alpha = -1.141 \pm 0.014$ and $\beta = -1.11 \pm 0.06$ [40]. The X-rays have a similar decay index of $\alpha = -1.1 \pm 0.1$ [87] and the optical/X-ray spectral index is

consistent with $\beta = -1.1$ [40]. Based on the radio to X-ray spectrum on day 12.1, Galama et al. [41] deduced that the cooling frequency is just below optical frequencies. At the optical and X-ray frequencies above the cooling frequency $\nu > \nu_c$, the observed value of α implies $p = 2.2$, which yields a spectral index β consistent with that observed for both the ISM and wind interaction models. Radio observations are crucial for distinguishing between these two models. In Fig. 1(a), we show the predictions of a wind interaction model at three wavelengths. They fit the radio data reasonably well, especially after about day 100 when the interstellar scintillation dies down [33]. In Fig. 1(b), we present an analytic fit to the R-band data, which is used in conjunction with the radio fit to obtain the best model parameters: $\epsilon_e = 0.2$, $\epsilon_B = 0.1$, $E_{52} = 0.3$, and $A_* = 0.3$. The inferred mass loss rate of $3 \times 10^{-6} M_\odot \text{ yr}^{-1}$ (for a wind speed of 10^3 km s^{-1}) is in the expected range of a Wolf-Rayet star. The optical afterglow brightens unexpectedly around day 2. Its temporal and spectral behaviors before day 2 are not explained by the wind model.

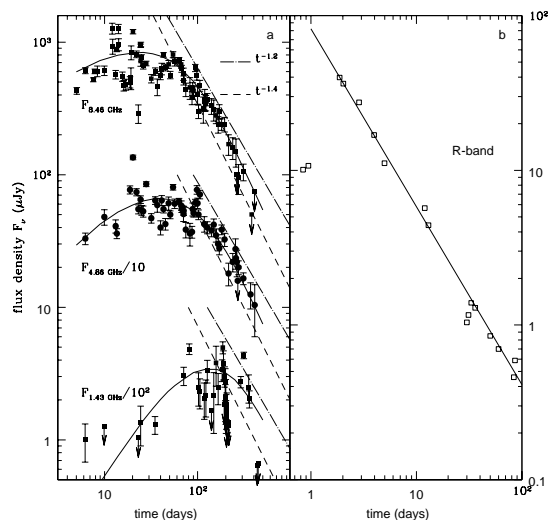


Fig. 1. Wind interaction model for the afterglow of GRB 970508 (adopted from Chevalier & Li [18]). Radio data are taken from Frail et al. [31,33] and R-band data from Sokolov et al. [109].

The peak flux F_{ν_m} and absorption frequency ν_a of GRB 970508 are inferred to decrease with time, which is consistent with the wind model but not with the standard spherical ISM model in the relativistic regime [40]. Frail et al. [33] discussed in depth these problems and suggested jet effects and a transition to non-relativistic expansion as possible solutions. They proposed three phases of evolution in a constant-density medium: a relativistic jet phase followed by a

phase of jet spreading, which is in turn followed by a phase of non-relativistic, spherical expansion. The jet spreading reduces the peak flux F_{ν_m} , and the emission expected from the non-relativistic phase is shown to be consistent with the radio data, although the complete model has yet to be calculated. The relatively slow decline of the optical afterglow for over 100 days [37] was unusual compared to other well-studied afterglows.

4.3 Jets, Winds, or Non-Relativistic Evolution?

Besides the four sources discussed above, there are half-dozen or so GRBs with reasonable multi-frequency coverage of afterglows, particularly at radio frequencies, which allows for detailed modeling. These include GRBs 980519, 991208, 991216, 000301C, 000418, 000926, and 010222 as of August 2001. The majority of these sources show clear steepening in the optical light curves (GRBs 991216, 000301C, 000926, and 010222), while in others the evidence for light curve steepening is weaker (GRBs 980519 and 991208) or absent (GRB 000418). A variety of models has been proposed for these sources. One common conclusion is that the simplest, standard model involving a relativistic spherical blast wave expanding into a constant-density medium is inadequate, and further refinements are necessary. GRB 000418 was modeled by Berger et al. [7], who found that both a spherical wind model and an ISM-interacting jet model fit the available radio-to-optical data reasonably well. For the remaining six sources, Panaitescu & Kumar [80,81,82] constructed semi-analytic jet models for both constant-density and wind-type ambient media. They found that ISM-interacting jet models can plausibly explain the broadband emission of all sources, and that wind-interacting jet models are compatible with the emission of GRBs 991208 and 991216 and can marginally accommodate the afterglows of GRBs 000301C and 010222 but cannot explain the observations of GRBs 980519 and 000926. Other authors have modeled these sources individually and, in some cases, come to different conclusions. We discuss these sources in turn.

GRB 980519 is one of three sources that show unusually steep light curve decay (with $\alpha < -2$) but weak or no evidence for breaks (the other two being GRBs 980326 and 991208). Chevalier & Li [17] proposed that the steep decay can be explained in a spherical wind model, provided that the electron energy index p is close to 3, a value that is higher than normally found in GRB afterglows but is within the range found in radio supernovae [13]. Radio data provide some support to this interpretation [34] but do not rule out the jet model, first advocated for this source by Sari et al. [105]. Indeed, Jaunsen et al. [57] have recently found some evidence for a sharp break in the R-band light curve, which they interpreted as due to a jet expanding into a wind-type medium. The relative sparseness of the data available around and after the break makes its identification less secure. If true, the sharpness of the break would be difficult to understand in a jet model, especially if the ambient medium is wind-like [62]. The spherical wind model of Chevalier & Li [17] did not take into account of inverse Compton scattering, which is important for the parameters they adopted (e.g., [103]).

Inverse Compton scattering lowers the cooling frequency, and poses a problem for the wind model in fitting the X-ray afterglow.

GRB 991208 is unique in that the radio data are sampled well enough to allow for a determination of the evolution of the characteristic frequencies ν_a and ν_m and the peak flux $F_{\nu, \max}$ at ν_m . The inferred scalings $\nu_a \propto t^{-0.15 \pm 0.23}$, $\nu_m \propto t^{-1.7 \pm 0.7}$ and $F_{\nu, \max} \propto t^{-0.47 \pm 0.20}$ [43] are compatible with the predictions of either the ISM-interacting jet model ($\nu_a \propto t^{-1/5}$, $\nu_m \propto t^{-2}$, and $F_{\nu, \max} \propto t^{-1}$) or the spherical wind model ($\nu_a \propto t^{-3/5}$, $\nu_m \propto t^{-3/2}$, and $F_{\nu, \max} \propto t^{-1/2}$) but not with those of the spherical ISM model ($\nu_a \propto t^0$, $\nu_m \propto t^{-3/2}$, and $F_{\nu, \max} \propto t^0$). Galama et al. [43] pointed out a problem with the wind model: the rate of optical light curve decline implies $p \geq 3.3$ and such a large value of p would be inconsistent with the radio-to-optical spectrum at day 7.3. The inconsistency motivated Li & Chevalier [66] to seek a model with a non-standard energy distribution of electrons. They found that a spherical wind model with a broken power-law electron energy distribution can reproduce all data as well as, if not better than, the jet model. Interestingly, in the jet model of Panaitescu & Kumar [81] for this source, where the jet dynamics is followed semi-analytically, the steep decay in optical is mostly attributed to a steepening in the electron energy distribution, as in the wind model for this source, rather than jet effects.

GRB 000301C was modeled by Li & Chevalier [66] using the same spherical wind model with an electron energy distribution that steepens at a certain (high) energy as the one applied to GRB 991208. The quality of the overall fit to the broad band radio-to-optical data is again comparable to that of an ISM-interacting jet model [5]. The radio data at 8.48 GHz are particularly well sampled for this source. The fact that its temporal decay (with $\alpha \approx -1.4$ [5]) is much shallower than that observed in R-band (with an asymptotic value of $\alpha \approx -2.7$) provides some evidence for a steepening of the electron energy distribution at high energies (see also [81]). The steepening in energy distribution produces a steepening in the optical light curves, which could mimic the jet effects. A difference is that the optical spectrum should steepen with time in the former case but not in the latter. Rhoads & Fruchter [99] presented IR-optical-UV data at several epochs, showing some evidence for spectral steepening with time. These data are fitted reasonably well by the wind model. The spectral steepening would be more pronounced in the optical to X-ray regime. Unfortunately, X-ray observations are not available for this source. Kumar & Panaitescu [63] attributed the steepening of the R-band light curve to a sudden large drop in the density of the ambient medium and Dai & Lu [27] to transition to non-relativistic evolution. The predictions of these models on radio emission remain to be worked out and compared with observations.

GRB 991216 is a source well observed in radio, optical and X-rays. The decay indexes at these wavelengths ($\alpha = -0.82 \pm 0.02$ at 8.46 GHz, -1.33 ± 0.01 at R-band and -1.61 ± 0.06 at 2–10 keV) are all different [35]. There is some evidence for light curve steepening at R-band, although the data at late times are too sparse to tightly constrain the time of transition from one power-law decay to another and the decay index after the transition [51]. The optical to X-ray data

are consistent with an ISM-interacting jet model [51], but the radio data are not [35]. Frail et al. [35] attributed the bulk of the radio emission to either the reverse shock as in GRB 991023 [104] or a second forward shock. Panaitescu & Kumar [80] examined the multi-frequency data, and concluded that all of the data can be fitted reasonably well using an ISM-interacting jet model, provided that a large curvature exists in the electron energy distribution, with p changing from ~ 1.2 to ~ 2.1 . GRB 991216 is therefore the third source (after GRBs 991208 and 000301C discussed above; see also [81]) for which a steepening in the electron energy distribution is proposed, although in all three cases the interpretation is model dependent.

GRB 000926 stands apart from other sources in that its X-ray afterglow is observed nearly two weeks after the explosion [90]. There is clear evidence for steepening in the optical light curves, with the decay index changing from $\alpha = -1.46 \pm 0.11$ to -2.38 ± 0.07 around 1.8 ± 0.1 days [53,91,39,100], pointing to a jet explanation. However, the decay after the break is significantly steeper than that in X-rays, estimated to be $\alpha = -1.89^{+0.19}_{-0.16}$ [90], which is difficult to explain in the standard jet model. Piro et al. [90] proposed an alternative model involving a mildly collimated blast wave expanding into a dense uniform medium ($n \sim 3 \times 10^4 \text{ cm}^{-3}$), with the transition to non-relativistic evolution occurring ~ 5 days after the explosion. Harrison et al. [53] showed that such a high density appears to have difficulties reproducing the radio data. They suggested that the standard jet model, either in a constant-density or wind-like medium, can fit the broad band data reasonably well, provided that the inverse Compton emission contributes significantly to the X-ray emission (see also [129] and [82]).

GRB 010222 is well observed in X-rays, with a decay index $\alpha = -1.33 \pm 0.04$ [56] that is nearly identical to that in the optical after a break around ~ 0.5 days (e.g., [69]). Before the break, the optical light curve is significantly flatter, with $\alpha \sim -0.6$ to -0.8 . The steepening of optical light curves can be interpreted as due to jet effects [111,101,22], provided that the electron energy distribution is very flat (with $p \sim 1.5$) as required by the asymptotic relation $p = -\alpha$ after the break [105]. This relation, originally derived for $p > 2$, may not be applicable to the case of $p < 2$ [4,24]. Masetti et al. [69] and in 't Zand et al. [56] favored an alternative model, in which the transition to non-relativistic evolution occurs rapidly in a very dense medium ($n \sim 10^6 \text{ cm}^{-3}$). The inferred $p \approx 2.2$ is more in line with those inferred for other GRBs (see however [81]). It is not clear, however, whether this high density model can reproduce the early radio detection of the source [6].

5 Discussion and Conclusions

No single model explains all of the dozen or so relatively well observed GRB afterglows. The model that comes closest appears to be the ISM-interacting jet model at the present time. It fits particularly well the multi-frequency data of GRBs 990123 and 990510. To reproduce the afterglow observations of GRBs 991208, 991216 and 000301C, a relatively flat electron energy distribution with

$p < 2$ is required; the flat distribution must steepen at high energies to $p > 2$ for the total electron energy to remain bound. The model also appears capable of describing the data of GRBs 000418 [7] and 000926, provided that inverse Compton scattering contributes significantly to the X-ray emission of the latter [53]. In addition, the steep decay of the optical light curves of GRBs 980326 and 980519 has been attributed to jet effects [105], and GRB 970508 has been modeled as a mildly collimated jet making a transition to a spherical non-relativistic evolution [33].

However, a number of the above sources can be modeled equally well or perhaps better by the wind-interacting spherical model. This is particularly true for GRB 970508. In the case of GRBs 991208 and 000301C, a non-standard electron energy distribution is required [66], as is the case for GRB 991216 (Li & Chevalier, in preparation). In addition, the wind model can fit the extensive radio data of GRB 980425/SN 1998bw, provided that a late energy injection occurs. Furthermore, the optical and X-ray afterglow data of GRB 970228 are compatible with the wind model, after the subtraction of plausible supernova emission from the optical light curve [93,42]. Frail et al. [32] searched for this source in radio for the first year, and did not detect any afterglow. The upper limits are of order 100 μ Jy or less at 8.46 GHz where the monitoring is most frequent. This absence of radio afterglow is not easy to explain in the standard, ISM-interacting spherical model, but is compatible with either a spherical wind model or ISM-interacting jet model [18], since in both models the peak flux decreases with frequency. The jet model may have difficulty with the relatively flat decay of the optical light curve ($\alpha \sim -1.6$) unless the electron energy distribution is very flat and/or the asymptotic slope after the jet break has yet to be reached. A relatively complete optical/IR data set also exists for GRB 980703 [9,11,55]. The inferred large extinction intrinsic to its bright host galaxy, coupled with the sparseness of the published X-ray [115] and radio data [9], makes it impossible to constrain models firmly.

The presence or absence of supernova emission in the optical afterglow may provide a powerful means for corroborating the ISM or wind model. The ISM-interacting sources are not expected to be accompanied by supernovae, and one indeed finds no evidence for supernova in the most probable ISM interactors: GRBs 990123 and 990510. The wind-interacting sources, on the other hand, are expected to be associated with supernovae, and the best wind interactors GRBs 980425 and 970508 are probably associated with supernovae. The evidence of supernova association is strong for GRB 980425, as reviewed by Galama and Iwamoto & Nomoto in this book. The evidence is weaker for GRB 970508, based mainly on a “shoulder” in the late time light curve at the I_c -band [108]; supernova emission is not clearly seen in the R-band [37]. In the case of another possible wind interactor, GRB 970228, evidence for supernova has been marshaled by Reichart [93] and Galama et al. [42]; the alternative explanation involving dust echoes [30] appears less likely [94], especially if the GRB progenitors are Wolf-Rayet stars instead of red supergiants [14]. Association with a supernova has also been proposed for other sources, including GRBs 980326 [10],

991208 [12], and possibly 000418 [59,28]. Their afterglow observations appear to be compatible with both the jet and wind models. In no source can the presence of a supernova be excluded definitively [39,23].

The expansion into a wind-type medium and the association with supernova would point to a massive star origin for GRBs. The massive star connection is indirectly supported by the analysis of optically dark bursts by Reichart [95], which indicates that the majority of GRBs may be tied to giant molecular clouds, the sites of massive star formation. The connection may be strengthened by the presence of possible Fe line emission in the X-ray afterglows of GRBs 970508 [88], 970828 [128] 991216 [89], and 000214 [2], which implies a substantial amount of circumburst material. We have discussed GRB 970508 as a wind interactor. GRBs 970828 and 000214, are optically dark, which is compatible with the idea that they are tied to giant molecular clouds and thus (indirectly) to massive stars. Their afterglow data are insufficient to constrain ambient interaction models. However, some models for the Fe lines require a large Fe mass and densities $\gtrsim 10^8 \text{ cm}^{-3}$ at $r \approx 10^{16} \text{ cm}$ [123,114], much larger than the densities inferred in afterglow models and than expected in the wind from a massive progenitor star. The distribution of the dense gas is asymmetric and it is not present along the line of sight to the GRB, which is the region probed by the afterglow emission. The strong angular variation of the density is surprising; in the supranova model [114], the supernova would be expected to affect the density along the line of sight. The required Fe mass would be greatly reduced if the lines come from a much denser region closer to the explosion center, as in the collapsar-bubble model of Mészáros & Rees [73].

The absence of supernova emission in the afterglows of GRBs 990123 and 990510 is consistent with their being ISM-interactors with compact star merger progenitors. It therefore appears that there are two types of burst progenitors, with GRBs 970508 and 980425 representing the best examples of one type, and GRBs 990123 and 990510 the other ([18], see also [67]). The possible presence of supernova emission in the optical afterglows of GRBs 970228, 980326, 991208, and 000418, coupled with the fact that their afterglows can be fitted by the wind model, plausibly put them in the massive star category. This assignment is weakened, however, by the fact that the afterglows of these sources can be fitted by the ISM-interacting jet model as well. For the other GRBs with relatively well observed afterglows, the progenitor types are even less certain.

The interpretation of GRB afterglows in terms of ambient interaction models is complicated by several major uncertainties. For the jet model, the angular distribution of matter and energy inside the jet is not clear and the hydrodynamics of the jet-ambient medium interaction remains uncertain. Numerical simulations are beginning to address these issues [50]. An open issue common to both the jet and wind models is the shape of the energy distribution of the radiative electrons. Fitting the afterglow data of several GRBs requires a curvature in the energy distribution. How the required curvature comes about is not understood. This problem is particularly severe for the cases that demand a flat distribution with $p < 2$. In such cases, the afterglow emission depends sensitively on the way

in which the energy distribution steepens at high energies, and the steepening has not been treated self-consistently. Another open issue is how the postshock energy is distributed among electrons, protons, and magnetic field. In addition, the spherical wind model faces an interesting dilemma: the wind model implies a massive star progenitor, and a collimated flow is expected if it must escape from the center of a star. To some extent, the spherical model can be justified by the slow apparent evolution of a jet in a wind [62,46]. It may also be possible that, upon passing through the star, the jet becomes uncollimated due to a sudden weakening of the lateral confinement.

We conclude that there is evidence for two types of GRB afterglows in different environments: a constant-density interstellar medium and a wind of possibly Wolf-Rayet star origin. The types are not immediately distinguishable partly because, at an age of a few days, the preshock wind density is comparable to an interstellar density. At an age of seconds to minutes, the preshock density is much higher for the wind case, which could make the types more distinguishable. Pair production in the ambient medium could substantially modify the afterglow emission. Its effects are expected to be far greater in the wind case than in the ISM case [112,70,4]. In addition, the large difference in density for the two cases at small distances from the center of explosion affects the dynamics of blast wave energization, and thus the prompt emission [104,18]. While some theoretical work has been done on the prompt and early afterglow emission, much more is needed. Hopefully, rapid follow-up observations of GRB afterglows, to be enabled by HETE-2 and SWIFT, would put tighter constraints on the ambient interaction models and the nature of GRB progenitors.

This work was supported in part by NASA grant NAG5-8130.

References

1. E. Amato, M. Salvati, R. Bandiera, F. Pacini, L. Woltjer: *A&A* **359**, 1107 (2000)
2. L.A. Antonelli, et al.: *ApJ* **545**, L39 (2000)
3. D. Bhattacharya: *Bull. Astr. Soc. India* **29**, 107 (2001)
4. A.M. Beloborodov: *ApJ*, submitted (astro-ph/0103321) (2001)
5. E. Berger, et al.: *ApJ* **545**, 56 (2000)
6. E. Berger, et al.: GCN No. 968 (2001)
7. E. Berger, et al.: *ApJ* **556**, 556 (2001)
8. R.D. Blandford, C.F. McKee: *Phys. Fluids* **19**, 1130 (1976)
9. J.S. Bloom, et al.: *ApJ* **508**, L21 (1998)
10. J.S. Bloom, et al.: *Nature* **401**, 453 (1999)
11. A.J. Castro-Tirado, et al.: *ApJ* **511**, L85 (1999)
12. A.J. Castro-Tirado, et al.: *A&A* **370**, 398 (2001)
13. R.A. Chevalier: *ApJ* **499**, 810 (1998)
14. R.A. Chevalier: Second Rome GRB Workshop (astro-ph/0102212) (2001)
15. R.A. Chevalier, C. Fransson: *ApJ* **558**, L27 (2001)
16. R.A. Chevalier, J.N. Imamura: *ApJ* **270**, 554 (1983)
17. R.A. Chevalier, Z.-Y. Li: *ApJ* **520**, L29 (1999)
18. R.A. Chevalier, Z.-Y. Li: *ApJ* **536**, 195 (2000)
19. J. Chiang, C.D. Dermer: *ApJ* **512**, 699 (1999)

20. E. Costa, et al.: *Nature* **387**, 783 (1997)
21. S. Covino, et al.: *A&A* **348**, L1 (1999)
22. R. Cowsik, T.P. Prabhu, G.C. Anupama, B.C. Bhatt, D.K. Sahu, S. Ambika, Padmakar, S.G. Bhargavi: *Bull. Astr. Soc. India*, in press (astro-ph/0104363) (2001)
23. S. Dado, A. Dar, A. De Rujula: preprint (astro-ph/0107367) (2001)
24. Z.G. Dai, K.S. Cheng: *ApJ* **558**, L109 (2001)
25. Z.G. Dai, T. Lu: *MNRAS* **298**, 87 (1998)
26. Z.G. Dai, T. Lu: *ApJ* **519**, L155 (1999)
27. Z.G. Dai, T. Lu: *A&A* **367**, 501 (2001)
28. A. Dar, A. De Rujula: preprint (astro-ph/0008474) (2000)
29. E. Ergma, E.P.J. van den Heuvel: *A&A* **331**, L29 (1998)
30. A.A. Esin, R.D. Blandford: *ApJ* **534**, L151 (2000)
31. D.A. Frail, S.R. Kulkarni, L. Nicastro, M. Feroci, G.B. Taylor: *Nature* **389**, 261 (1997)
32. D.A. Frail, S.R. Kulkarni, D.S. Shepherd, E. Waxman: *ApJ* **502**, L119 (1998)
33. D.A. Frail, E. Waxman, S.R. Kulkarni: *ApJ* **537**, 191 (2000)
34. D.A. Frail, et al.: *ApJ* **534**, 559 (2000)
35. D.A. Frail, et al.: *ApJ* **538**, L129 (2000)
36. D.A. Frail, et al.: *ApJ*, submitted (astro-ph/0108436) (2000)
37. A.S. Fruchter, et al.: *ApJ* **545**, 664 (2000)
38. C.L. Fryer, S.E. Woosley, D.H. Hartmann: *ApJ* **526**, 152 (1999)
39. J.U. Fynbo, et al.: *A&A* **373**, 796 (2001)
40. T.J. Galama, et al.: *ApJ* **497**, L13 (1998)
41. T.J. Galama, R.A.M.J. Wijers, M. Bremer, P.J. Groot, R.G. Strom, C. Kouveliotou, J. van Paradijs: *ApJ* **500**, L97 (1998)
42. T.J. Galama, et al.: *ApJ* **536**, 185 (2000)
43. T.J. Galama, et al.: *ApJ* **541**, L45 (2000)
44. G. García-Segura, N. Langer, M.-M. MacLow: *A&A* **316**, 133 (1996)
45. G. Ghisellini, D. Lazzati: *MNRAS* **309**, L7 (1999)
46. L.-J. Gou, Z.G. Dai, Y.F. Huang, T. Lu: *A&A* **368**, 464 (2001)
47. J. Granot, T. Piran, R. Sari: *ApJ* **527**, 236 (1999)
48. J. Granot, T. Piran, R. Sari: *ApJ* **534**, L163 (2000)
49. J. Granot, R. Sari: preprint (astro-ph/0107009) (2001)
50. J. Granot, M. Miller, T. Piran, W.-M. Suen, P.A. Hughes: 2nd Rome GRB Workshop (astro-ph/0103038) (2001)
51. J.P. Halpern, et al.: *ApJ* **543**, 697 (2000)
52. F.A. Harrison et al.: *ApJ* **523**, L121 (1999)
53. F.A. Harrison et al.: *ApJ* **559**, 123 (2001)
54. S. Holland, G. Björnsson, J. Hjorth, B. Thomsen: *A&A* **364**, 467 (2000)
55. S. Holland, et al.: *A&A* **371**, 371 (2001) 0703
56. J.J.M. in 't Zand, et al.: *ApJ*, in press (astro-ph/0104362) (2001)
57. A.O. Jaunsen, et al.: *ApJ* **546**, 127 (2001)
58. J.I. Katz: *ApJ*, **422**, 248 (1994)
59. S. Kloze, et al.: *ApJ*, **545**, 271 (2000)
60. S.R. Kulkarni, et al.: *Nature* **395**, 663 (1998)
61. S.R. Kulkarni, et al.: *Nature* **398**, 389 (1999)
62. P. Kumar, A. Panaitescu: *ApJ* **541**, L9 (2000)
63. P. Kumar, A. Panaitescu: *ApJ* **541**, L51 (2000)
64. E. Kuulkers, et al.: *ApJ* **538**, 638 (2000)
65. Z.-Y. Li, R.A. Chevalier: *ApJ* **526**, 716 (1999)

66. Z.-Y. Li, R.A. Chevalier: *ApJ* **551**, 940 (2001)
67. M. Livio, E. Waxman: *ApJ* **538**, 187 (2000)
68. A.I. MacFadyen, S.E. Woosley, A. Heger: *ApJ* **550**, 410 (2001)
69. N. Masetti, et al.: *A&A* **374**, 382 (2001)
70. P. Mészáros, E. Ramirez-Ruiz, M.J. Rees: *ApJ* **554**, 660 (2001)
71. P. Mészáros, M.J. Rees: *ApJ* **476**, 232 (1997)
72. P. Mészáros, M.J. Rees: *MNRAS* **306**, L39 (1999)
73. P. Mészáros, M.J. Rees: *ApJ* **556**, L37 (2001)
74. P. Mészáros, M.J. Rees, R.A.M.J. Wijers: *ApJ* **499**, 301 (1998)
75. M.R. Metzger, et al.: *Nature* **387**, 878 (1997)
76. R. Moderski, M. Sikora, T. Bulik: *ApJ* **529**, 151 (2000)
77. B. Paczyński: *ApJ* **494**, L45 (1998)
78. A. Panaitescu: *ApJ* **556**, 1002 (2001)
79. A. Panaitescu, P. Kumar: *ApJ* **543**, 66 (2000)
80. A. Panaitescu, P. Kumar: *ApJ* **554**, 667 (2001)
81. A. Panaitescu, P. Kumar: *ApJ* **560**, L49 (2001)
82. A. Panaitescu, P. Kumar: *ApJ*, submitted (astro-ph/0109124) (2001)
83. A. Panaitescu, P. Mészáros: *ApJ* **501**, 772 (1998)
84. A. Panaitescu, P. Mészáros, M.J. Rees: *ApJ* **503**, 315 (1998)
85. E. Pian, et al.: *A&A* **372**, 456 (2001)
86. T. Piran, J. Granot: Second Rome GRB meeting (astro-ph/0107009) (2001)
87. L. Piro, et al.: *A&A* **331**, L41 (1998)
88. L. Piro, et al.: *ApJ* **514**, L73 (1999)
89. L. Piro, et al.: *Science* **290**, 955 (2000)
90. L. Piro, et al.: *ApJ* **558**, 442 (2001)
91. P.A. Price, et al.: *ApJ* **549**, L7 (2001)
92. E. Ramirez-Ruiz, L.M. Dray, P. Madau, C.A. Tout: *MNRAS*, submitted (astro-ph/0012396) (2000)
93. D.E. Reichart: *ApJ* **521**, L111 (1999)
94. D.E. Reichart: *ApJ* **554**, 643 (2001)
95. D.E. Reichart: *ApJ* submitted (astro-ph/0107546) (2001)
96. J.E. Rhoads: *ApJ* **487**, L1 (1997)
97. J.E. Rhoads: *ApJ* **525**, 737 (1999)
98. J.E. Rhoads: Ninth Marcel Grossman Meeting (astro-ph/0103028) (2001)
99. J.E. Rhoads, A.S. Fruchter: *ApJ* **546**, 117 (2001)
100. R. Sagar, S.B. Pandey, V. Mohan, D. Bhattacharya, A.J. Castro-Tirado: *Bull. Astr. Soc. India* **29**, 1 (2001) 0926
101. R. Sagar, et al.: *Bull. Astr. Soc. India* **29**, 91 (2001) 0222
102. R. Sari: *ApJ* **524**, L43 (1999)
103. R. Sari, A.A. Esin: *ApJ* **548**, 787 (2001)
104. R. Sari, T. Piran: *ApJ* **517**, L109 (1999)
105. R. Sari, T. Piran, J.P. Halpern: *ApJ* **519**, L17 (1999)
106. R. Sari, T. Piran, R. Narayan: *ApJ* **497**, L17 (1998)
107. P.M. Solomon: in *Starburst Galaxies: Near and Far* (astro-ph/0101482) (2001)
108. V.V. Sokolov: Second Rome GRB Workshop (astro-ph/0102492) (2001)
109. V.V. Sokolov, A.I. Kopylov, S.V. Zharikov, M. Feroci, L. Nicastro, E. Palazzi: *A&A* **334**, 117 (1998)
110. K.Z. Stanek, P.M. Garnavich, J. Kaluzny, W. Pych, I. Thompson: *ApJ* **522**, L39 (1999)
111. K.Z. Stanek, et al.: *ApJ*, in press (astro-ph/0104329) (2001)

112. C. Thompson, P. Madau: ApJ **538**, 105 (2000)
113. J. van Paradijs, et al.: Nature **386**, 686 (1997)
114. M. Vietri, G.Ghisellini, D. Lazzati, F. Fiore, L. Stella: ApJ **550**, L43 (2001)
115. P.M. Vreeswijk, et al.: ApJ **523**, 171 (1999)
116. E. Waxman: ApJ **485**, L5 (1997)
117. E. Waxman: ApJ **489**, L33 (1997)
118. E. Waxman, A. Loeb: ApJ **515**, 721 (1999)
119. D.M. Wei, T. Lu: ApJ **505**, 252 (1998)
120. D.M. Wei, T. Lu: ApJ **541**, 203 (2000)
121. D.M. Wei, T. Lu: preprint (astro-ph/0107371) (2001)
122. K. Weiler, N. Panagia, M. Montes: ApJ, in press (astro-ph/0106131) (2001)
123. C. Weth, P. Mészáros, T. Kallman, M.J. Rees: ApJ **534**, 581 (2000)
124. R.A.M.J. Wijers, T.J. Galama: ApJ **523**, 177 (1999)
125. R.A.M.J. Wijers, M.J. Rees, P. Mészáros: MNRAS **288**, L51 (1997)
126. R.A.M.J. Wijers, et al.: ApJ **523**, L33 (1999)
127. S.E. Woosley: ApJ **405**, 273 (1993)
128. A. Yoshida, et al.: A&AS **138**, 433 (1999)
129. S.A. Yost, et al.: Second Rome GRB Workshop (astro-ph/0107556) (2001)